Clinical Radiology 74 (2019) 78.e23–78.e30

Contents lists available at ScienceDirect

Clinical Radiology

journal homepage: www.clinicalradiologyonline.net

Differentiation of focal organising pneumonia and peripheral adenocarcinoma in solid lung lesions using thin-section CT-based radiomics

T. Zhang [a], M. Yuan [a], Y. Zhong [a], Y.-D. Zhang [a], H. Li [b], J.-F. Wu [c], T.-F. Yu [a,*]

[a] Department of Radiology, The First Affiliated Hospital of Nanjing Medical University, Nanjing, 210029, China
[b] Department of Pathology, The First Affiliated Hospital of Nanjing Medical University, Nanjing, 210029, China
[c] GE Healthcare, Shanghai, 210000, China

ARTICLE INFORMATION

Article history:
Received 7 March 2018
Accepted 28 August 2018

AIM: To evaluate the predictive role of radiomics based on computed tomography (CT) in discriminating focal organising pneumonia (FOP) from peripheral lung adenocarcinoma (LA).

MATERIALS AND METHODS: Institutional research board approval was obtained for this retrospective study. One hundred and seventeen patients with FOP and 109 patients with LA who underwent thin-section CT from January 2011 to August 2017 were reviewed systematically and analysed. The clinical and radiological features were established as model A and multi-feature-based radiomics as model B. The diagnostic performance of model A, model B, and model A+B were evaluated and compared via receiver operating characteristic (ROC) curve analysis and logistic regression analysis.

RESULTS: Sex, symptoms, necrosis, and the halo sign were identified as independent predictors of LA. The area under the ROC curve (Az value), accuracy, sensitivity, and specificity of model A were 0.839, 75.7%, 82.6%, and 69.2% respectively. Model B showed significantly higher accuracy than model A (83.6% versus 75.7%, p=0.032). The top four best-performing features, WavEnLH_s-3, WavEnHH_s-3, Teta3, and Volume, performed as independent factors for discriminating LA. Regression analysis indicated that model B had superior model fit than model A with Akaike information criterion (AIC) values of 73.6% versus 59.1%, respectively. Combining model A with model B is useful in achieving better diagnostic performance in discriminating FOP from LA: the Az value, accuracy, sensitivity, and specificity were 0.956, 87.6%, 85.3%, and 89.7% respectively.

CONCLUSIONS: Radiomics based on CT exhibited better diagnostic accuracy and model fit than clinical and radiological features in discriminating FOP from LA. Combination of both achieved better diagnostic performance.

© 2018 The Royal College of Radiologists. Published by Elsevier Ltd. All rights reserved.

Introduction

For the first time in 1983, organising pneumonia (OP) was described to be the reparative inflammatory response of lung tissue with various aetiologies, including infection, drug toxicity, and organ transplantation, etc.[1] Focal OP

* Guarantor and correspondent: T.-F. Yu, Department of Radiology, the First Affiliated Hospital of Nanjing Medical University, 300, Guangzhou Road, Nanjing, Jiangsu Province, 210029, China. Tel.: +86 138 1381 0516.
E-mail address: njmu_ytf@163.com (T.-F. Yu).

https://doi.org/10.1016/j.crad.2018.08.014
0009-9260/© 2018 The Royal College of Radiologists. Published by Elsevier Ltd. All rights reserved.

(FOP), which is a unique subtype of OP, accounting for 10–15% of OP, may present as a solitary nodule or mass in the lungs.[2] Some FOP cases are difficult to distinguish from peripheral lung cancer (LC),[3,4] as they share similar radiological features, such as solid nodules or masses with lobulation, spiculation, pleural retraction, or vascular convergence. Zheng *et al.* showed that there was no specific radiological manifestation to distinguish FOP from LC by comparing the computed tomography (CT) findings of 20 cases of FOP and 40 cases of LC.[3] Thus, unnecessary pulmonary segmentectomy or lobectomy may be performed in patients with FOP, instead of short-term observation and repeat CT imaging.

Various diagnostic techniques, including invasive and non-invasive methods, can be used to discriminate FOP from LC. Invasive methods include transbronchial lung biopsy or percutaneous puncture biopsy (PPB) by ultrasound or CT. Among them, CT-guided PPB is the most commonly used method; however, as an invasive examination, a series of contraindications and complications limit its application; massive haemoptysis or arterial air embolism rarely occur, but may lead to serious consequences that can be fatal.[5,6] One of the most important non-invasive methods is 2-[^{18}F]-fluoro-2-deoxy-D-glucose positron-emission tomography (FDG-PET). Kagna *et al.* showed that an SUVmax of 2.5 as the threshold value for separating benign from malignant lesions had a sensitivity of 81.2%; however, with a specificity of only 50%.[7] Yurdanur *et al.* demonstrated that the SUVmax value of FOP reached 6.72, which is inconsistent with the threshold SUVmax of 2.5.[8] The unsatisfactory diagnostic performance and inconsistent results showed that ^{18}F-FDG PET could not be considered as a prognostic factor in distinguishing FOP from LC (Fig 1).

In recent years, radiomics have undergone considerable development. Using automated data characterisation algorithms, the imaging data of a volume of interest (VOI) can be transformed into high-dimensional quantitative descriptors for analysis. The multi-feature-based radiomics can be extracted to reveal the heterogeneity of tumours and to evaluate the comprehensive characterisation of underlying tumour phenotypes.[9–11] FOP and LC have completely different biological behaviours, pathologic processes, and internal spatial construction. It was hypothesised that multi-feature-based radiomics may be able to discriminate FOP from LC.

Lung adenocarcinoma (LA) is the most commonly seen pathological type in peripheral LC. Therefore, the purpose of the present study was to evaluate the diagnostic performance of CT-based radiomics in discriminating FOP from LA, and to compare it with the clinical and radiological features based model.

Materials and methods

Patients

This retrospective study was approved by the institutional review board with a waiver of written informed consent. Five hundred and twelve patients with LA and 267 patients with OP who underwent thin-section CT from January 2011 to August 2017 were reviewed and analysed systematically. All of the OP cases in the study are primary OP, which is found without another primary disease and not as a minor finding of another disease.[12] Patients who met with the following criteria were enrolled: (a) pathological results were confirmed by surgical resection or CT-guided percutaneous biopsy; (b) preoperative non-enhanced thin-section CT was performed; (c) all lesions manifested as solid solitary nodules or masses on the CT images; (d) no chemotherapy or radiation therapy was undertaken before surgery; (e) clinical data were available, including age, sex, smoking history, clinical symptoms (the specific symptoms are listed in Table 1), weight loss, and history of chronic obstructive pulmonary disease (COPD). Central lung cancers are mainly located at the inner field of the lung adjacent to the hilus and have an ill-defined boundary, which are significantly different from OP, so central lung cancers were excluded from the study.

A total of 109 patients with LA and 117 patients with FOP were finally enrolled in this study and 553 patients were excluded with at least one of the following criteria: (a) lesions manifested as non-solid, part-solid, or non-nodular forms (n=386); (b) two or more lesions were founded in the same patient's CT images (n=116); (c) unsatisfactory imaging quality due to respiratory motion artefact during the examination (n=38); (d) CT-guided percutaneous biopsy was performed before the thin-section CT scan (n=45).

CT

All patients underwent non-enhanced thoracic CT using a 128-section (SOMATOM Definition AS+; Siemens, Malvern, PA, USA) CT system with the following settings: 1 mm section thickness and 0.8 mm reconstruction interval, 120 kVp, and CareDose current selection for radiation reduction. All images were reconstructed with a high-kernel (b60) and a high-resolution 512×512 matrix.

Imaging analysis

The entire-tumour VOI was automatically segmented using MM oncology lungCAD software in Syngo.Via, Version VA30. The precise edge of the VOI was manually adjusted by two thoracic radiologists (author 1 and author 3 with 6 and 3 years of experience in thoracic imaging), if necessary. Then author 2 with 10 years of experience in thoracic imaging rechecked it to ensure the accuracy of segmentation.

Two thoracic radiologists, who performed the VOI adjusting and were blinded to the pathological diagnosis, interpreted the CT images in consultation. CT features, including location, spiculation, necrosis, lymphadenopathy, air bronchogram, halo sign, and calcification were read with both lung (window width, 1,500 HU; window level, −600 HU) and mediastinal (window width, 500 HU; window level, 50 HU) window settings. Image interpretation results were also rechecked by author 2.

A total of 298 radiomic features were extracted from segmented VOIs delineated previously, by using Analysis Kit

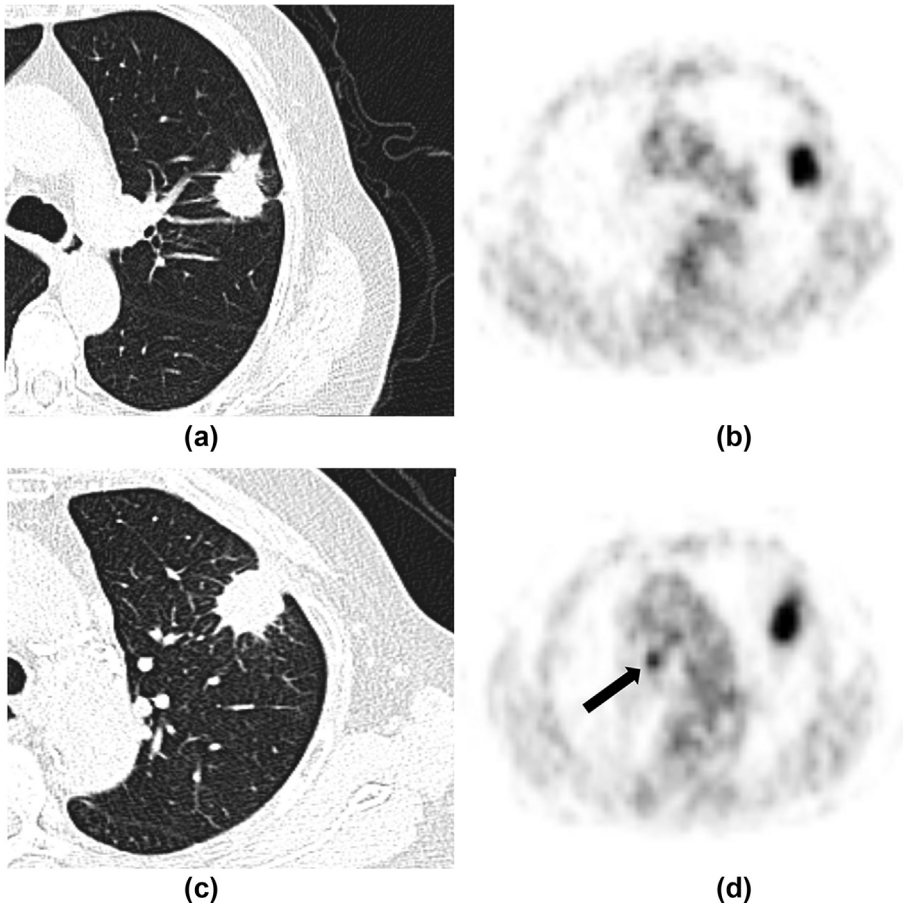

Figure 1 A 81-year-old woman with a diagnosis of FOP. (a,b) A peripheral lung adenocarcinoma was detected accidentally in a 67-year-old woman without obvious symptoms. A lobulate nodule with spiculate margins located in the upper lobe of left lung was seen. PET/CT showed increased FDG uptake with SUVmax 5.3. (c,d) A similar nodule located in the upper lobe of the left lung demonstrated similar radiological features and increased FDG uptake (SUVmax: 7). An enlarged mediastinal lymph node (SUVmax: 4.9) was observed at the same imaging level (arrow).

software, Version 3.0 (GE Healthcare, Shanghai, China). In brief, the radiomic features were divided into three groups: (I) tumour intensity features, illustrated the histogram of intensity value, are first-order level radiomic features, which represent surface texture of the tumour and include parameters such as variance, skewness, kurtosis, and percentiles (Analysis Kit Software have 19 9ercentiles, 5–95%); (II) texture, derived from the grey-level co-occurrence matrix (GLCM) at five interpixel distances: 1, 2, 3, 4, and 5 (angular second moment, contrast, correlation, entropy, sum entropy, sum of squares, sum average, sum variance, inverse different moment, difference entropy, difference variance) and run length matrices (GLRLM) at four angles: 0°, 45°, 90°, and 135° (run-length non-uniformity, grey-level non-uniformity, long run emphasis, short run emphasis, fraction of image in runs) and absolute gradient (gradient mean, variance, skewness, kurtosis, and percentage of pixels with non-zero gradient), autoregressive model (teta 1–4, sigma); (III) wavelet features, consisted of both intensity and textural features based on a wavelet decomposition from the tumour image (WAV: energies[En] of wavelet transform coefficients in frequency channels LL, HL, HH, and LH, abbreviated as WavEnLL, WavEnHL, WavEnHH, and WavEnLH, WAV features were calculated for four scaling factors [s=1–4]).[13,14]

Features were selected based on reproducibility and redundancy to reduce the feature dimension. Firstly, the concordance correlation coefficient (CCC) was calculated to test the reproducibility and stability of each feature and CCC values $\geq$0.9 were kept. Secondly, linear correlation method was used to calculate the correlations among the rest stable radiomics features. The redundant features with correlation $>$0.9 were removed.

Model development and classification

Two predictive models were constructed for the following analysis. In the first model (model A: clinical and radiological features), 14 input parameters i.e. age, sex, smoking history, symptom, weight loss history, COPD history, lesion diameter, location, spiculation, necrosis, lymphadenopathy, air bronchogram, halo sign, and calcification were used as input variables. In the second model (model B), radiomics features were used as input factors.

Table 1
Clinical and radiographic characteristics and univariate analysis of patients.

Characteristics	FOP	LA	χ^2	*t*-Value	*p*-Value
Number of patients	117	109			
Age (year)	60.21±11.15	62.73±9.45		−1.827	0.069
Sex (male/female)	92/25	46/63	31.499		0.000
Smoking history (yes/no)	41/76	22/87	6.197		0.013
Weight loss history (yes/no)	9/108	11/98	0.403		0.526
Symptomatic (yes/no)	89/28	39/70	37.295		0.000
Fever (%)	27.4 (27/117)	2.8 (3/109)			
Expectoration (%)	54.7 (64/117)	13.8 (15/109)			
Haemoptysis (%)	9.4 (11/117)	0.9 (1/109)			
Chest pain (%)	14.5 (17/117)	4.6 (5/109)			
Dry cough (%)	0.0 (0/117)	15.6 (17/109)			
Physical examination (%)	23.9 (28/117)	64.2 (70/109)			
COPD history (yes/no)	18/99	13/96	0.570		0.450
Lesion diameter (cm)	3.39±1.60	2.98±1.06		2.281	0.024
Lesion location (upper/middle and lower)	54/63	50/59	0.002		0.966
Spiculation (yes/no)	86/31	73/36	1.154		0.283
Necrosis (yes/no)	29/88	3/106	20.764		0.000
Lymphadenopathy (yes/no)	12/105	16/93	1.017		0.313
Air bronchogram (yes/no)	33/84	39/70	1.491		0.222
Halo sign (yes/no)	31/86	7/102	16.257		0.000
Calcification (yes/no)	6/111	2/107	0.958		0.328

Unless otherwise indicated, data are mean ± standard deviation.
FOP, focal organising pneumonia; LA, lung adenocarcinoma; COPD, chronic obstructive pulmonary disease.

A robust recursive feature elimination (RFE) method based on support vector machine (SVM) was used for feature selection. The feature with the lowest ranking score (contribution weight ω) by recursively training on RFE-SVM was removed until the cumulative ω of all desired features reached 80%.

The features selected by RFE-SVM were then classified by SVM using a radical basis function (RBF) kernel for separating the labelled training data into two classes using the following equation.

$$f(x) = \sin\left\{\sum_{i=1}^{k}\alpha_i^* y_i K(x\cdot x_i) + b^*\right\}$$

where α was calculated as:

$$\max_{\alpha} \sum_{i=1}^{n}\alpha_i - \frac{1}{2}\sum_{i,j=1}^{n}\alpha_i\alpha_j y_i y_j K(x\cdot x_i)$$

$$\text{s.t.},\ \alpha_i \geq 0,\ i = 1,\ldots,n$$

$$\sum_{i=1}^{n}\alpha_i y_i = 0$$

$K(x, x_i)$ represents the kernel function of RBF kernel and is described as:

$$K(x, x_i) = \exp\left(-\gamma|x - x_i|^2\right)$$

As the relatively small sample size, SVM classifiers were trained (cohort 1) and validated (cohort 2) using the repeated (five repeat iterations) and leaving-one-out fivefold cross-validation approach. All examples except onefold for validation, the other fourfolds were applied for training. This procedure was repeated until all the examples in the database were used once in the validation cohort. The workflow for machine learning algorithms was illustrated in Fig 2.[15]

Feature stability was tested in the training phase according to the method by Aerts *et al.* using the publicly available RIDER data set.[10] The stability ranks were compared for test–retest by two radiologists who delineated lesions on CT images from 20 patients. The stability of features in the repeated experiment was measured by the test–retest concordance correlation coefficient (CCC_{TreT}).

Statistical analysis

Continuous variables including age, maximum diameter of lesions accorded with normal distribution and homogeneity of variance were compared by *t*-test. The differences of categorical variables, such as sex and smoking history, were analysed using the χ^2 test.

The performance of two predictive models were analysed using a receiver operating characteristic (ROC) regression analysis. The diagnostic sensitivity, specificity, accuracy, and area under the ROC curve (AUC) were calculated at a cut-off value in context of the maximum of the Youden index. The ROC curves were compared and estimated by using MedCalc statistical software (version 8.2.0.1, MedCalc Software, Mariakerke, Belgium).

The multivariable regression analysis was used to evaluate the predictive performance of model A and model B in the validation cohort after modelling by SVM. Akaike information criterion (AIC) in χ^2 analysis was used to determine the best-fit model.

p-Values of <0.05 were considered to indicate a statistically significant difference. All these statistical analyses were performed using IBM SPSS Statistics, version 22.0 (SPSS Inc., Chicago, IL, USA).

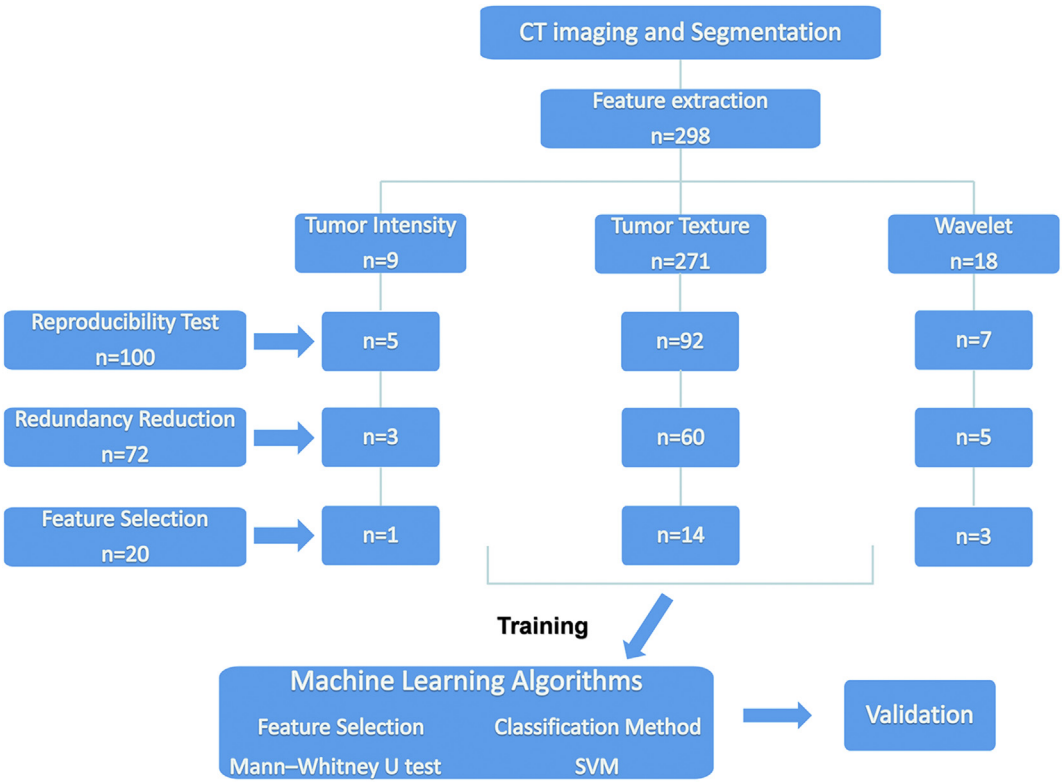

Figure 2 Analysis workflow. A total of 298 radiomic features were extracted from VOIs delineated on CT images. After feature selection, SVM classifiers were trained (cohort 1) and validated (cohort 2) by using the repeated (five repeat iterations) and leaving-one-out cross-validation approach.

Results

Clinical and radiological findings

Two hundred and twenty-six patients were enrolled in the study (138 men, mean age 60.6±10.7 years; 88 women, mean age 62.8±9.8 years). Among them, 109 patients (48.2%) were diagnosed with LA, and 117 patients (51.8%) with FOP. Male patients (78.6% versus 42.2%, $p<0.001$), with smoking history (35% versus 20.2%, $p=0.013$) and clinical symptoms (76.1% versus 35.8%, $p<0.001$) occurred more often in FOP than LA. Lesions in FOP were significantly larger than LA with the longest diameters of 3.39±1.6 versus 2.98±1.06 cm ($p=0.024$).

With regard to radiological features, necrosis and the halo sign occurred more often in FOP (24.8% versus 2.8%; 26.5% versus 6.4%, $p<0.001$, respectively). No significant differences were found in lesion location, spiculation, lymphadenopathy, air bronchogram, and calcification. The details are listed in Table 1.

In model A, sex (OR=0.171, $p<0.001$), symptomatic (OR=0.153, $p<0.001$), necrosis (OR=0.141, $p=0.007$), and the halo sign (OR=0.342, $p=0.034$) were identified as independent factors to predict the probability of LA (Table 2).

Construction of the radiomic score

The test–retest concordance correlation coefficient revealed a significant correlation ($CCC_{TreT}=0.926$, $p<0.001$), which demonstrated the stability of radiomic features and the reproducibility of the radiomic metrics.

The top 18 radiomics features are listed in Table 3 and Fig 3 based on the contribution weight of each feature by RFE-SVM analysis with the total weights of 82.1%. The four best-performing radiomics features: WavEnLH_s-3, WavEnHH_s-3, Teta3 and Volume were showed to be independent factors in discriminating malignant lesions (Table 4). A radiomics score (RAD-score), which was generated by calculating the optimum cut-off value of the integrating weights of multiple features by SVM was 0.920.

Model comparison

Prediction factors for the probability of LA in model A was generated as follows:

$$p = e^x/(1+e^x)$$

Table 2
Independent predictors in the multivariate logistic regression analyses and the odd ratios.

Factor	Regression coefficient	Standard error	*p*-Value	Odds ratio (95% confidence interval)
Sex	−1.766	0.360	0.000	0.171 (0.084–0.346)
Symptomatic	−1.880	0.352	0.000	0.153 (0.076–0.304)
Necrosis	−1.960	0.722	0.007	0.141 (0.034–0.580)
Halo sign	−1.073	0.506	0.034	0.342 (0.127–0.922)
Constant	2.410	0.383	0.000	11.131

Table 3
Category of representative features (n=18).

Category	Representative features
C1: Tumour intensity (n=1)	Perc. 90%
C2: Tumour texture (n=14)	S(0,2)SumAverg; S(1,1)SumAverg; S(0,1)SumAverg; S(3,0)SumAverg; S(3,3)SumAverg; _Area_S(0,4); _Area_S(0,3); _Area_S(4,0); _Area_S(3,0); _Area_S(2,0); 135dr_RLNonUni; 45dgr_RLNonUni; Volume; Teta3
C3:Wavelet (n=3)	WavEnLL_s-4; WavEnHH_s-3; WavEnLH_s-3

Perc. 90%, Percentile 90%; S(x,y), grey level co-occurrence matrix for inter-pixel distance x along rows and y along columns; SumAverg, sum average; 135dr_RLNonUni, 135 degree run-length non-uniformity; 45dgr_RLNonUni, 45 degree run-length non-uniformity; WavEnLL(HH,LH), energies of wavelet transform coefficients in frequency channels LL, HH, and LH.

where x = 2.410 + (−1.766 × sex) + (−1.880 × symptomatic) + (−1.960 × necrosis) + (−1.073 × halo sign); e is the natural logarithm. Male is scored as 1 and female as 0, symptomatic is scored as 1 or otherwise as 0; necrosis and halo sign are both derived from the assessment on CT images (1: yes, 0: no).

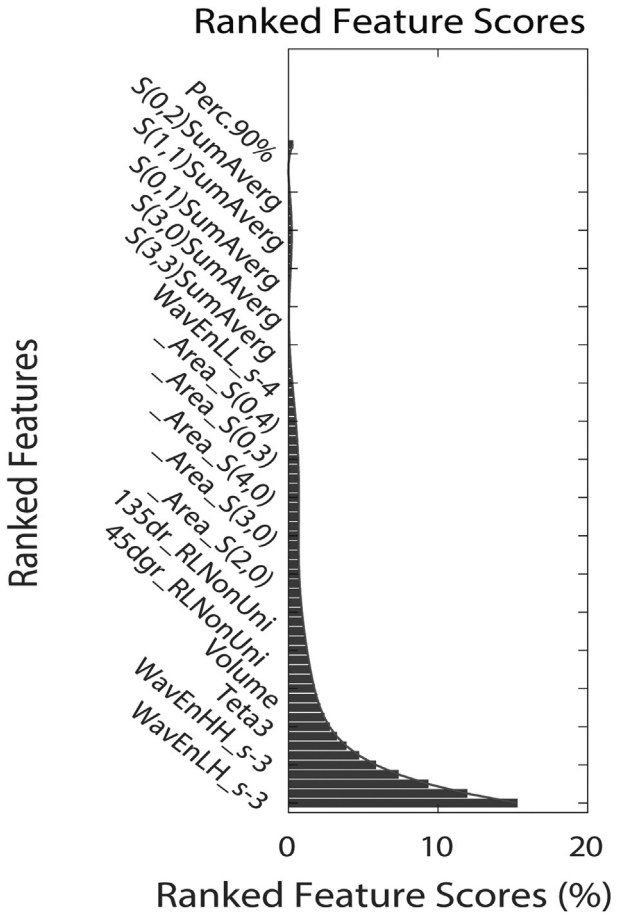

Figure 3 The contributions of the top 18 best radiomics features according to RFE-SVM. The total weights (the area under curve) were 82.1% when accumulating these top 18 features.

The Az value, accuracy, sensitivity, and specificity of model A were 0.839, 75.7%, 82.6% and 69.2% respectively. The AIC value of model A was 59.1%.

The predictive performance of model B based on radiomics showed significantly improved over model A in accuracy (83.6% versus 75.7%) and model fit (AIC value 73.6% versus 59.1%; Fig 4).

Combining model A with model B is useful in achieving a better diagnostic performance in discriminating FOP from LA, the Az value, accuracy, sensitivity, and specificity were 0.956, 87.6%, 85.3%, and 89.7% respectively.

Table 4 demonstrated that none of the four best-performing radiomic features could be used to successfully stratify patients into high-risk and low-risk groups by means of Wilcoxon signed-rank test.

Discussion

The present study demonstrated that a newly developed model B based on radiomics exhibited better diagnostic accuracy and model fit than model A (clinical and radiological features) in discriminating FOP from LA, with accuracies of 83.6% versus 75.7% and AIC values of 73.6% versus 59.1%, respectively. Combining model A with model B is useful in achieving better diagnostic performance.

In the present study, a series of clinical and radiological features were analysed and generated as model A for differentiating LA from FOP. FOP occurred more often in male patients. Patients with clinical symptoms had a tendency to have FOP, whilst no tendency in LA. The result was consistent with previous studies.[4,16,17]

With regard to radiological features, there were significant differences in the presence of necrosis and the halo sign between FOP and LA, which was consistent with the findings of Wu *et al.*[18] The most likely explanation is that the inflammatory injury of FOP usually results in inflammatory debris filling the alveoli and dilatation of local vessels, as well as central liquefaction necrosis. Although the growth of LA is a relatively slow process that involves “sustained angiogenesis” and “resisting cell death”,[19] in which degeneration is common but significant necrosis is rare.[16,20] The halo sign is another useful independent predictor for discriminating FOP from LA, which is consistent with the study by Zhao *et al.*[4] The halo sign was usually present in FOP due to chronic inflammatory cell infiltration. A previous study[21] found that LA may also show halo signs because of tumour infiltration, but it is mainly seen in invasive adenocarcinoma appearing as mixed ground-glass nodules. The interfaces of the tumour—lung in most lesions are clear.[22]

In the present study, two predictive models were constructed and compared based on clinical and radiological features (model A) and radiomics (model B). Model B showed significant improvement in diagnostic accuracy and model fit in predicting LA. Multi-feature-based radiomics can be extracted to reveal tumour heterogeneity and to evaluate the comprehensive characterisation of underlying tumour phenotypes,[9–11] which plays a potential role in personalised

Table 4
Effectiveness of the model A, model B and model A+B in diagnosis of FOP and LA.

Analysis model	FOP (n=117)	LA (n=109)	p-Value	Cut-off value	Accuracy (%)	Az	SEN (%)	SPE (%)	Model-fitting information	
									AIC (%)	R^2 value
Model A	0.31±0.25	0.66±0.23	0.000	>0.611	75.7	0.839	82.6	69.2	59.1	0.346
Model B	−0.65±0.46	0.48±0.58	0.000	>−0.270	83.6	0.920	76.7	90.0	73.6	0.541
WavEnLH_s-3	38.97±21.77	52.25±27.48	0.000	>50.354		0.646	50.5	76.9		
WavEnHH_s-3	10.10±6.68	12.73±7.04	0.004	>10.605		0.637	56.9	67.5		
Teta3	0.184±0.221	0.267±0.256	0.009	>0.267		0.591	48.6	69.2		
Volume	1570.71±1343.51	1158.23±889.44	0.007	≤1787		0.582	84.4	35.0		
Model A+B	0.78±0.58	−0.73±0.61	0.000	≤0.009	87.6	0.956	85.3	89.7	78.6	0.615

Az, area under the receiver operating curve; SEN, sensitivity; SPE, specificity; FOP, focal organising pneumonia; LA, lung adenocarcinoma; AIC, Akaike information criterion.

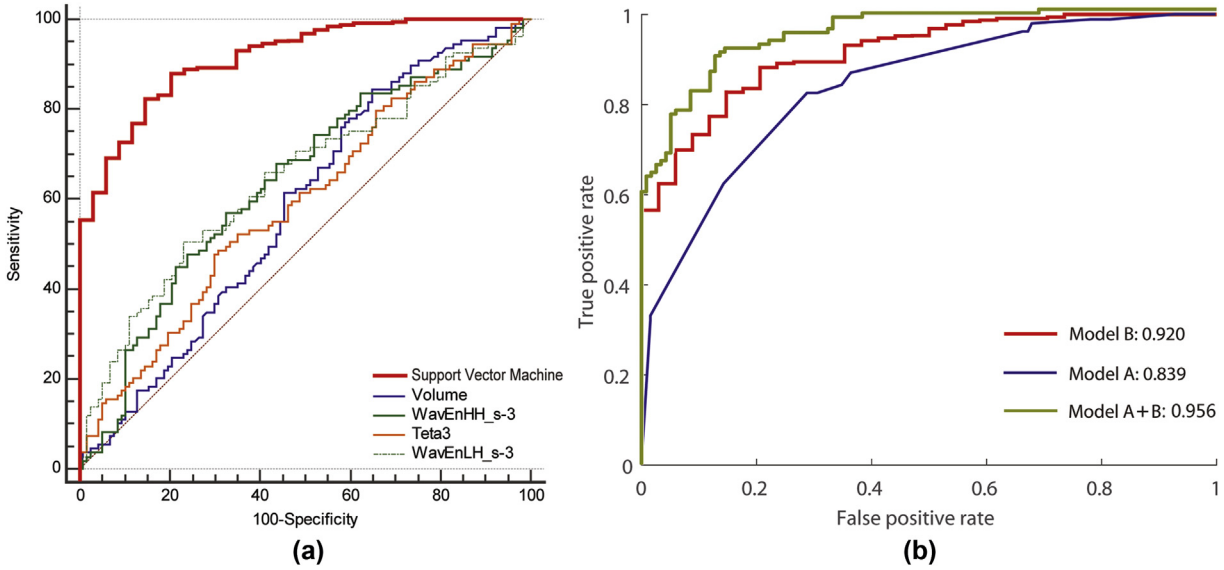

Figure 4 (a) ROC analysis of radiomics (model B) and top four best-performing features for distinguishing FOP from LA. (b) ROC analysis of the predictive model A, radiomics model B, and model A+B for distinguishing FOP from LA.

diagnosis and personalised medicine.[23] FOP and LA have completely different biological behaviours, pathologic processes, and internal spatial construction. Thus, multi-feature-based radiomics may be able to discriminate FOP from LA. The present study demonstrated that radiomics showed satisfactory diagnostic performance with the accuracy of 83.6% in differentiating FOP from LA, which showed significant improvement when compared with model A.

The four best-performing radiomic features were WavEnLH_s-3, WavEnHH_s-3, Teta3, and Volume. Similar to candidate genomics, it is difficult to discriminate these two groups using single radiomics-based factors. Multiple radiomics-based factors could provide a more comprehensive and robust approach.

There are some limitations in the present study. Firstly, an external validation was absent because of relative small sample size. Second, FOP is initiated by lung injury, which is commonly associated with a wide variety of infectious diseases, while some non-infectious diseases, such as drug toxicity, collagenosis, even unknown aetiological causes, may also result in FOP. Because all of the FOP cases in the present study are primary OP, which is found without another primary disease and not as a minor finding of another disease, the pathologies are not all clear and the clinical symptoms of FOP are varied; thus a classification for FOP was not conducted according to the pathologies, and also because of the relative small sample size. More samples are needed in order to further improve and perfect the present research. Thirdly, the CT images evaluated in the present study were unenhanced, it is not known whether contrast-enhanced CT will affect the result, but in order to avoid indeterminate results, patients who underwent contrast-enhanced CT were excluded. Further study is needed to compare the results of non-enhanced CT and contrast enhanced CT and evaluate the impact of contrast-enhanced CT on analysis results.

Conflicts of interest

The authors declare no conflict of interest.

References

1. Drakopanagiotakis F, Paschalaki K, Abu-Hijleh M, *et al*. Cryptogenic and secondary organizing pneumonia: clinical presentation, radiographic findings, treatment response, and prognosis. *Chest* 2011;**139**(4):893–900.

2. Baque-Juston M, Pellegrin A, Leroy S, *et al*. Organizing pneumonia: what is it? A conceptual approach and pictorial review. *Diagn Interv Imaging* 2014;**95**(9):771–7.
3. Zheng Z, Pan Y, Song C, *et al*. Focal organizing pneumonia mimicking lung cancer: a surgeon's view. *Am Surg* 2012;**78**(1):133–7.
4. Zhao F, Yan SX, Wang GF, *et al*. CT features of focal organizing pneumonia: an analysis of consecutive histopathologically confirmed 45 cases. *Eur J Radiol* 2014;**83**(1):73–8.
5. Hare SS, Gupta A, Goncalves ATC, *et al*. Systemic arterial air embolism after percutaneous lung biopsy. *Clin Radiol* 2011;**66**(7):589–96.
6. Cheng HM, Chiang KH, Chang PY, *et al*. Coronary artery air embolism: a potentially fatal complication of CT-guided percutaneous lung biopsy. *Br J Radiol* 2010;**83**(988):e83–5.
7. Kagna O, Solomonov A, Keidar Z, *et al*. The value of FDG-PET/CT in assessing single pulmonary nodules in patients at high risk of lung cancer. *Eur J Nucl Med Mol Imaging* 2009;**36**(6):997–1004.
8. Yurdanur E, Berna AÖ, Özmen Özlem, *et al*. The evaluation of FDG PET/CT scan findings in patients with organizing pneumonia mimicking lung cancer. *Mol Imaging Radionucl Ther* 2015;**24**(2):60–5.
9. Lambin P, Rios-Velazquez E, Leijenaar R, *et al*. Radiomics: extracting more information from medical images using advanced feature analysis. *Eur J Cancer* 2012;**48**(4):441–6.
10. Aerts HJWL, Velazquez ER, Leijenaar RTH, *et al*. Decoding tumour phenotype by noninvasive imaging using a quantitative radiomics approach. *Nat Commun* 2014;**5**:4006.
11. Yamamoto S, Korn RL, Oklu R, *et al*. ALK molecular phenotype in non-small cell lung cancer: CT radiogenomic characterization. *Radiology* 2014;**272**(2):568–76.
12. Tokgöz Akyýl F, Aðca M, Mýsýrlýoðlu A, *et al*. Organizing pneumonia as a histopathological term. *Turk Thorac J* 2017;**18**:82–7.
13. Coroller TP, Grossmann P, Hou Y, *et al*. CT-based radiomic signature predicts distant metastasis in lung adenocarcinoma. *Radiother Oncol* 2015;**114**(3):345–50.
14. Aerts HJWL, Grossmann P, Tan Y, *et al*. Defining a radiomic response phenotype: a pilot study using targeted therapy in NSCLC. *Sci Rep* 2016;**6**:33860.
15. Parmar C, Grossmann P, Bussink J, *et al*. Machine learning methods for quantitative radiomic biomarkers. *Sci Rep* 2015;**5**:13087.
16. Chu ZG, Sheng B, Liu MQ, *et al*. Differential diagnosis of solitary pulmonary inflammatory lesions and peripheral lung cancers with contrast-enhanced computed tomography. *Clinics* 2016;**71**(10):555–61.
17. Huo Z, Feng R, Tian X, *et al*. Clinicopathological findings of focal organizing pneumonia: a retrospective study of 37 cases. *Int J Clin Exp Pathol* 2015;**8**(1):511–6.
18. Wu CT, Chang YL, Chen WC, *et al*. Surgical treatment of organising pneumonia mimicking lung cancer: experience of 27 patients. *Eur J Cardio-Thoracic Surg* 2010;**37**(4):797–801.
19. Hanahan D, Weinberg RA. Hallmarks of cancer: the next generation. *Cell* 2011;**144**(5):646–74.
20. Li Y, Yang ZG, Chen TW, *et al*. First-pass perfusion imaging of solitary pulmonary nodules with 64-detector row CT: comparison of perfusion parameters of malignant and benign lesions. *Br J Radiol* 2010;**83**(993):785–90.
21. Parrón M, Torres I, Pardo M, *et al*. The halo sign in computed tomography images: differential diagnosis and correlation with pathology findings. *Arch Bronconeumol* 2008;**44**(7):386–92.
22. Hashimoto M, Miyauchi T, Heianna J, *et al*. Accurate diagnosis of peripheral small cell lung cancer with computed tomography. *Tohoku J Exper Med* 2009;**217**(3):217–21.
23. Yoon HJ, Sohn I, Cho JH, *et al*. Decoding tumor phenotypes for ALK, ROS1, and RET fusions in lung adenocarcinoma using a radiomics approach. *Medicine (Baltimore)* 2015 Oct;**94**(41):e1753.